Charge Disproportionation and Voltage-Induced Metal–Insulator Transitions Evidenced in β-$Pb_xV_2O_5$ Nanowires

Peter M. Marley, Adam A. Stabile, Chun Pui Kwan, Sujay Singh, Peihong Zhang, G. Sambandamurthy, and Sarbajit Banerjee**

The roster of materials exhibiting metal–insulator transitions with sharply discontinuous switching of electrical conductivity close to room temperature remains rather sparse, despite the fundamental interest in the electronic instabilities manifested in such materials and the plethora of potential technological applications ranging from frequency-agile metamaterials to electrochromic coatings and Mott field-effect transistors. Here, unprecedented, pronounced metal-insulator transitions induced by application of a voltage are demonstrated for nanowires of a vanadium oxide bronze with intercalated divalent cations, β-$Pb_xV_2O_5$ ($x \approx 0.33$). The induction of the phase transition through application of an electric field at room temperature makes this system particularly attractive and viable for technological applications. A mechanistic basis for the phase transition is proposed based on charge disproportionation evidenced at room temperature in near-edge X-ray absorption fine structure (NEXAFS) spectroscopy measurements, ab initio density functional theory calculations of the band structure, and electrical transport data, suggesting that transformation to the metallic state is induced by melting of specific charge localization and ordering motifs extant in these materials.

1. Introduction

Strongly correlated materials are characterized by a combination of spatially and temporally inhomogeneous charge and spin localization and fluctuation motifs.[1] A characteristic signature of most correlated materials is the facile accessibility of different electronic states, giving rise to particularly fecund electronic phase diagrams featuring various incongruous regions such as quantized spin states, charge density waves, and superconducting, charge-ordered, and correlated metallic regimes.[2] Minor structural perturbations can substantially modify the phase stabilities given the intimate coupling between lattice and orbital degrees of freedom in these systems, and the existence of several nearly degenerate states.[1c] Spatial confinement such as induced by scaling to nanoscale dimensions can induce structural distortions or perturb charge ordering to a sufficient extent to induce substantial alterations of phase stabilities and to manifest dramatic phase transformations. In this regard, mixed-valence vanadium oxide bronzes with the general formula $M_xV_2O_5$ (where M: alkali, alkaline earth, and transition metal cations) have long seemed to be ideal model systems for exploration of correlation effects and electron–phonon coupling in quasi-1D geometries.[3] The relative insensitivity of the V_2O_5 frameworks to cation occupancies in the tunnel sites of classical Wadsley β and β' phases further qualify these materials for examination of a wide range of compositional stoichiometries and the influence of said stoichiometry variation on chemical bonding, electronic transport, and magnetic coupling.[2b,4]

Despite the conceptual promise of these materials, realization of their full potential and exploration of intrinsic correlation effects have long been stymied by the sensitivity of the electronic phase diagrams to precise cation stoichiometry.[5] The presence of point defects along the quasi-1D tunnels gives rise to random potentials that can severely degrade metallic character and cause convolution of electronic transport data with Anderson's weak localization, defect migration, and other defect-mediated non-intrinsic phenomena. Careful preparation of high-quality macroscopic single crystals has permitted a tantalizing glimpse of the possibilities available upon fine tuning compositional and stoichiometric parameters in these materials with perhaps the most spectacular example being the induction of superconductivity under high pressure adjacent to charge-ordered states observed in β-$Na_{0.33}V_2O_5$, β-$Ag_{0.33}V_2O_5$, β'-$Cu_{0.65}V_2O_5$, and β/β'-$Li_{0.33}V_2O_5$. Charge ordering and modest thermally induced metal–insulator transitions have also been noted for divalent cation counterparts β-$Sr_{0.33}V_2O_5$ and β-$Ca_{0.33}V_2O_5$ although no consensus has emerged regarding the appropriate site occupancies and doping ratios required to trigger metal–insulator transitions or superconductivity.

P. M. Marley, Prof. S. Banerjee
Department of Chemistry
University at Buffalo
The State University of New York
Buffalo, NY 14260-3000, USA
E-mail: sb244@buffalo.edu

A. A. Stabile, C. P. Kwan, S. Singh, Prof. P. Zhang, Prof. G. Sambandamurthy
Department of Physics
University at Buffalo
The State University of New York
Buffalo, NY 14260–1500, USA
E-mail: sg82@buffalo.edu

DOI: 10.1002/adfm.201201513

In recent work, we have demonstrated that by preparing the vanadium bronzes in nanostructured form through low-temperature hydrothermal synthesis, deviations from perfect stoichiometry are avoided through the fortunate circumstance of self-purification wherein defects migrate to surfaces of nanostructures, yielding almost perfectly single-crystalline slabs of material that can be reproducibly fabricated.[6,7] Intriguingly, controlling cation stoichiometry and manipulating the electronic phase diagrams at the nanoscale has enabled us to observe up to six-orders-of-magnitude colossal metal–insulator transitions at temperatures in the 300–400 K regime for 1D nanowires of δ-$K_xV_2O_5$ and β'-$Cu_xV_2O_5$.[7b,7c]

Herein, we describe a synthetic route to 1D nanowires of β-$Pb_{0.33}V_2O_5$, a vanadium bronze with polarizable divalent Pb^{2+} cations (bearing lone pairs of s electrons), and evidence sharply discontinuous metal–insulator transitions under the influence of an electric field. The marked difference between bulk and nanoscale behavior further underlines the benefits of interrogating these materials approaching the single-domain limit and makes for a rare addition to the roster of materials exhibiting a pronounced electrically tunable metal–insulator transition at room temperature.

2. Results and Discussion

2.1. Structural Aspects of β-$Pb_{0.33}V_2O_5$

The β-phase of $Pb_{0.33}V_2O_5$ crystallizes in the monoclinic space group $C2/m$ and comprises three crystallographically distinctive vanadium atoms: $V(1)O_6$ octahedra that share edges are arrayed in a zig-zag chain, $V(2)O_6$ octahedra share corners constituting an infinite ladder-like chain, and $V(3)O_5$ square pyramids share edges to constitute another zig-zag-type chain; all three infinite chains are aligned parallel to the *b*-axis and enclose infinite open tunnels along the same direction (**Figure 1**a). The Pb^{2+} cations reside at interstitial sites within the tunnel framework and upon incorporation reduce a fraction of V^{5+} sites to V^{4+}. In the ground state, electron localization and charge disproportionation are extant along the length of the quasi-1D tunnels and the material can be viewed as being on the insulating side of a Mott transition.[4b,8] Unlike the β-phase vanadium bronzes containing monovalent cations or even its divalent Ca^{2+} and Sr^{2+} counterparts, the thermally induced transport observed for single crystals of β-$Pb_xV_2O_5$ shows only a modest discontinuity from insulating to metallic behavior, which has been

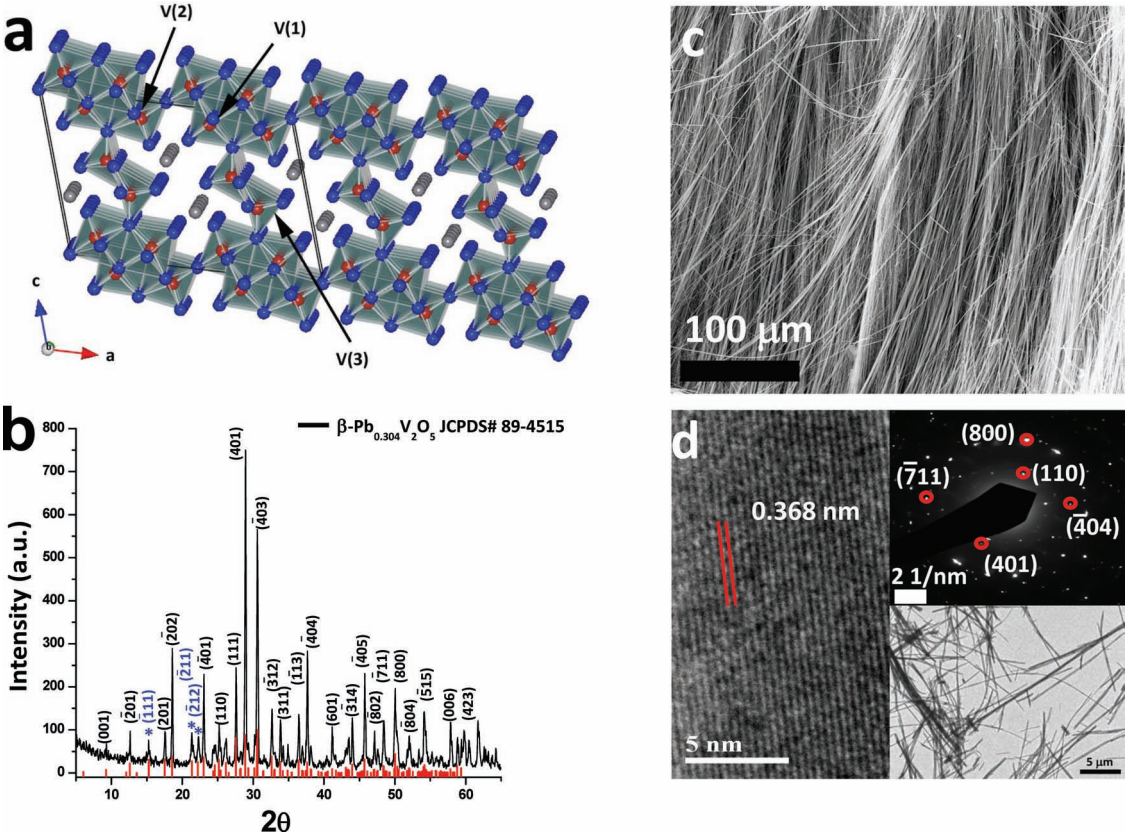

Figure 1. a) Crystal structure of monoclinic β-$Pb_{0.33}V_2O_5$. The three distinct vanadium polyhedra are depicted with vanadium atoms (red) coordinated to oxygen (blue). Lead atoms occupying interstitial tunnel sites are shown in grey. b) XRD pattern of the as-prepared nanowires indexed to β-$Pb_{0.304}V_2O_5$ (JCPDS #41-1426), the blue asterisk and reflections correspond to superstructure reflections indicating bidimensional periodicity of the intercalated Pb^{2+} cations. c) Panoramic SEM image of the nanowires illustrating the high purity of the synthesis and the >100 μm lengths of the nanowires. d) HRTEM image depicting the crystalline nature of the nanowires, the inset shows a low-magnification TEM image of numerous nanowires and a SAED pattern acquired for several nanowires indexed to β-$Pb_{0.304}V_2O_5$.

attributed thus far to poor crystal quality and weak localization of the electrons on the vanadium chains.[9] The fabrication of single-crystalline β-$Pb_{0.33}V_2O_5$ nanowires permits transport measurements of this material without obscuration from defect migration and dynamics.

2.2. Synthesis and Characterization of β-$Pb_{0.33}V_2O_5$ Nanowires

Nanowires of β-$Pb_xV_2O_5$ were synthesized via the hydrothermal reaction of lead acetate $Pb(CH_3COO)_2.3H_2O$ (Fluka) and V_2O_5 powder (Sigma Aldrich). Stoichiometric amounts were placed in a Teflon-lined acid digestion vessel (Parr) along with 16 mL of H_2O (ρ = 18.2 MΩ/cm) and heated in a sealed autoclave at 250 °C for 72 h. The resulting product was then vacuum filtered and washed with copious amounts of water and allowed to dry in air. Details of instrumentation and experimental conditions used to characterize the samples are presented in the Experimental Section. Near-edge X-ray absorption fine structure (NEXAFS) and X-ray absorption near-edge structure (XANES) spectroscopy data were collected on National Institute of Standards and Technology beamlines U7A and X23A2, respectively, at the National Synchrotron Light Source of Brookhaven National Laboratory.

Figure 1b shows the powder X-ray diffraction pattern measured for the as-prepared nanowires. The pattern can be indexed to phase-pure β-$Pb_{0.304}V_2O_5$ (Joint Committee on Powder Diffraction Standards (JCPDS) #89-4515) with additional reflections (denoted by an asterisk and reflections indicated in blue) corresponding to a periodic superstructure constituted from ordering of Pb^{2+} ions along two dimensions: a) along the length of the tunnel wherein the cations constitute a zig-zag chain parallel to the crystallographic *b*-axis, along with b) alternating arrays of ordered and disordered chains along the crystallographic *a* axis.[11] Mentre et al. have observed such bidimensional superstructure formation only for high crystalline quality samples at stoichiometries $x > 0.3$ for β-$Pb_xV_2O_5$.[11] A SEM image illustrating the morphology, high aspect ratios, and high purity of the nanowires is shown in Figure 1c. The nanowires clearly range in length up to hundreds of microns. The diameter distribution has been deduced from low-magnification TEM images (inset to Figure 1d) and is centered around ≈170 nm, indicating aspect ratios well over 500. The prepared nanowires are single crystalline as indicated in Figure 1d, which depicts a lattice-resolved HRTEM image of an individual nanowire with a spacing of 0.368 nm that corresponds well to the separation between the (400) planes of β-$Pb_{0.33}V_2O_5$; this image also illustrates the *b*-axis is parallel to the length of the nanowire. The selected-area electron diffraction pattern of several nanowires is depicted in the inset to Figure 1d and can be again indexed to the β-phase of $Pb_{0.304}V_2O_5$. Chemical analysis via energy dispersive X-ray spectroscopy has confirmed a Pb concentration, $x = 0.31$, close to the stoichiometric limit of $x \approx 0.33$ for the β phase.

2.3. Electronic Structure of β-$Pb_{0.33}V_2O_5$

The electronic structure of the as-prepared β-$Pb_{0.33}V_2O_5$ nanowires has been examined by NEXAFS spectroscopy. NEXAFS spectroscopy involves the excitation of core electrons to partially filled or unoccupied states and the lineshapes and peak positions of elemental-edge-specific NEXAFS spectra reflect the unoccupied density of states (UDOS) of a solid-state compound (as modified by interaction with the created core-hole).[10] To first approximation, V L-edge spectra represent the d-projected UDOS and the O K-edge spectra represent the p-projected UDOS; hybridization of O 2p states with V3d levels allows for the observation of these transitions in the NEXAFS spectra. **Figure 2**a juxtaposes V L-edge and O K-edge NEXAFS data of bulk monoclinic VO_2, bulk V_2O_5, and β-$Pb_xV_2O_5$ nanowires. The two broad peaks at ≈520 and ≈526 eV correspond to the V L_{III} and V L_{II} edge resonances, respectively, and can be ascribed to transitions from $V2p_{3/2} \rightarrow V3d$ and $V2p_{1/2} \rightarrow V3d$, respectively. The O K-edge arises from transitions from O 1s core states to the O 2p levels hybridized with V3d orbitals; the pronounced splitting at the O K-edge reflects the crystal field splitting of V $3d_{x2-y2}$ and V $3d_{z2}$ (e_g*) states that are involved in direct V–O σ overlaps and the V $3d_{xy}$, $3d_{yz}$, and $3d_{xz}$ (t_{2g}*) states that participate in sideways V–O π bonding.[7a,7b,10b] The splitting of the e_g* and t_{2g}* hybridized states (Δ_2) for β-$Pb_xV_2O_5$ has been determined to be 2.2 eV, which is identical to that of δ-$K_{0.5}V_2O_5$ and slightly smaller than the 2.4 eV value measured for β'-$Cu_{0.65}V_2O_5$.[7a,7b] The O-and V-projected density of states calculated and plotted in **Figure 3** confirms the two distinctive regimes (t_{2g}* and e_g*) at the O K-edge. The close similarities in crystal field splitting attest to the analogous local V–O bonding within the quasi-1D V_2O_5 frameworks. In contrast, the splitting (Δ_1) at the V L_{III} edge is 1.9 eV. The sharp difference between the Δ_1 and Δ_2 values observed for β-$Pb_xV_2O_5$ suggests that the splitting of the V L_{III} feature cannot be explained based on crystal field considerations alone. Moreover, a DFT calculation shows that the three symmetry inequivalent vanadium atoms (V1, V2, and V3 in Figure 1a) have similar coordination environments, and consequently do not give rise to distinctive NEXAFS resonances that are as much as 1.9 eV apart in energy.[8,14] Instead, the distinctive splitting at the V L_{III} and O K-edges is averred to be a result of charge disproportionation and electron localization wherein discrete V^{4+} sites (reduced by accepting electrons from Pb^{2+} cations) are arrayed along the quasi-1D tunnels amidst the mostly V^{5+} V_2O_5 structural framework. Note that the results suggest charge disproportionation with distinctive electron densities on vanadium atoms that could be more complex than simple V^{4+}/V^{5+} ordering. The precise charge ordering pattern remains to be determined and is likely very distinct for each quasi-1D β/β' vanadium oxide bronze depending upon the size and polarizability of the intercalated cations, the ordering motif of the cations, and the degree of covalency of M–O interactions within the tunnel.

XANES spectra at the V K-edge are also rich with information about oxidation state and the local symmetry of the vanadium atom. Figure 2b shows V K-edge spectra for bulk orthorhombic V_2O_5, monoclinic VO_2, and β-$Pb_xV_2O_5$ nanowires; a distinctive pre-edge feature, absorption edge, and the primary 1s → 4p transition are observed. The pre-edge feature arises from transitions from 1s core levels to unoccupied V3d states that are rendered dipole-allowed due to mixing with p states upon departure from perfectly octahedral symmetry; accordingly, symmetric VO (rock salt structure and octahedral vanadium coordination) has no pre-edge absorption, whereas

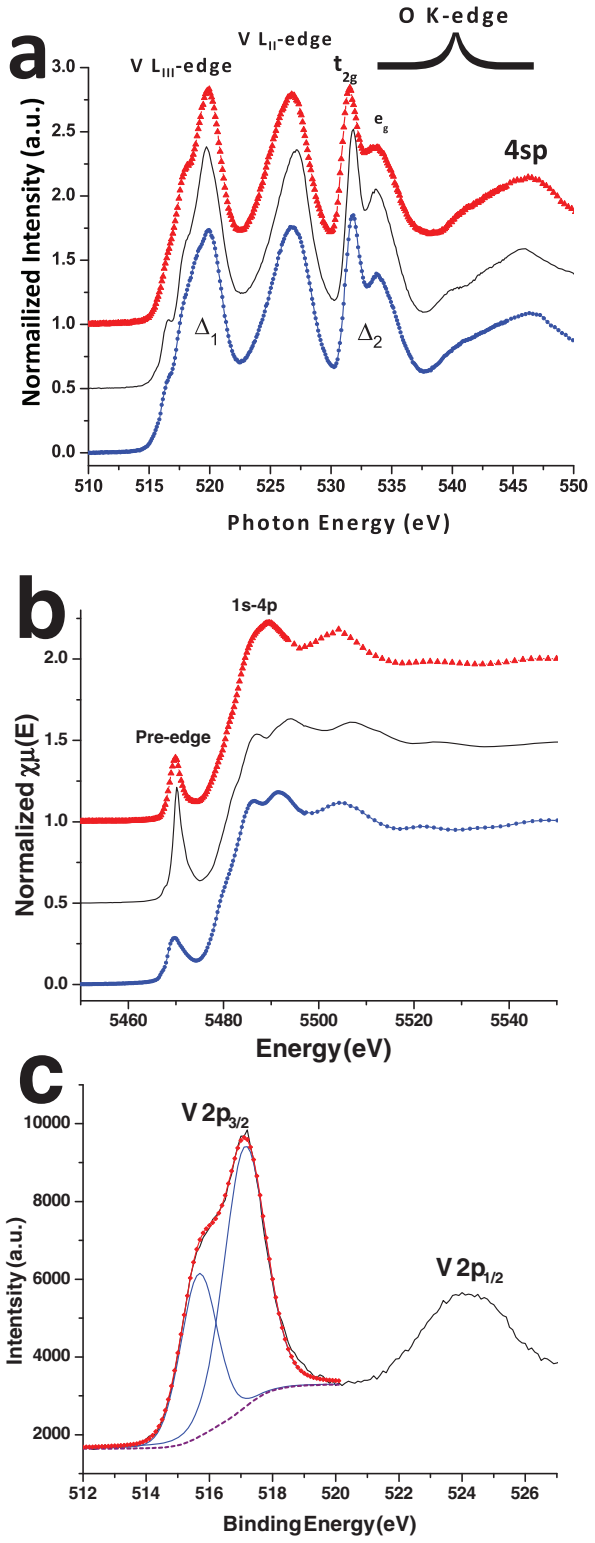

Figure 2. a) V L-edge and O K-edge NEXAFS specra of bulk V_2O_5 (solid black line), VO_2 (blue squares), and β-$Pb_xV_2O_5$ nanowires (red triangles). The difference in splitting between the V L_{III} (Δ_1) and O K (Δ_2) edges suggests charge disproportionation. b) Vanadium K-edge XANES spectra of bulk V_2O_5 (solid black line), VO_2 (blue squares), and β-$Pb_xV_2O_5$ nanowires (red triangles). c) High-resolution XPS spectrum acquired at the V 2p edge for β-$Pb_xV_2O_5$ nanowires (solid black line).

the strongly distorted vanadium-centered square pyramids of V_2O_5 yield a pronounced absorption feature (Figure 2b).[14] The relative intensity and peak position of the pre-edge feature for β-$Pb_xV_2O_5$ nanowires is intermediate between the square pyramid of V_2O_5 and the distorted octahedra of V_2O_4, which is expected from the distinctive symmetries of VO_6 octahedra and VO_5 square pyramids of the β-phase. The absorption edge feature, following Kunzl's law, also shows a monotonic dependence of peak position with oxidation state.[14a] The absorption edge features for β-$Pb_xV_2O_5$, V_2O_5, and V_2O_4 are 5481.8, 5482.3, and 5481.0 eV, respectively, indicating partial reduction of V^{5+} upon Pb incorporation and an intermediate oxidation state between V^{4+} and V^{5+}.

X-ray photoelectron spectroscopy (XPS) has further been performed to characterize the β-$Pb_xV_2O_5$ nanowires. Figure 2c shows high resolution V 2p spectra of the nanowires, the V $2p_{1/2}$ and V $2p_{3/2}$ peaks are observed at energies of 524 eV and 517.5 eV, yielding a spin-orbit splitting of 6.5 eV. Furthermore, the broadening and peak multiplicity of the V 2p region can be attributed to partial reduction of the V_2O_5 framework to V^{4+} at specific V sites upon incorporation of Pb. Peak fitting analysis of the V $2p_{3/2}$ absorption feature clearly shows two distinct vanadium contributions at 515.6 and 517.0 eV arising from distinct V^{4+} and V^{5+} oxidation states, respectively, which provides an approximate $V^{4+}/(V^{4+}+V^{5+})$ ratio of 0.30, close to the expected 0.33 ratio for divalent cations with $x = 0.33$ (some surface V^{4+} sites may be susceptible to oxidation in the nanowires). A redox titration has further been performed to determine the oxidation state of vanadium using the methodology described by Niwa et al.[13] From the titrations, a $V^{4+}/(V^{4+}+V^{5+})$ ratio of 0.294 ± 0.17 is deduced illustrating partial reduction of the V_2O_5 upon incorporation of Pb analogous to the conclusions derived from the XPS measurements.

Figure 3 shows the calculated total and atom-projected density of states (DOS) for β-$Pb_{0.33}V_2O_5$. Interestingly, the DOS is characterized by the manifestation of an in-gap state that is well-separated from the conduction and valence bands. V_2O_5 has an analogous split-off conduction band but notably the in-gap state in β-$Pb_{0.33}V_2O_5$ lies below the Fermi level and further has contributions from V 3d mixed with O 2p and Pb 6s (lone pair) states unlike in V_2O_5, wherein the split-off state is almost entirely V 3d in character. In past polarized NEXAFS spectroscopy results, we have shown that the split-off conduction band in V_2O_5 is primarily d_{xy} in origin.[10c] Ma et al. have calculated the DOS for analogous β-$Na_{0.33}V_2O_5$, which interestingly does not show a characteristic in-gap state.[8] From the joint DOS plotted in Figure 3, stoichiometric β-$Pb_{0.33}V_2O_5$ is a metal with a DOS maxima located at the Fermi level, which is indeed characteristic of electronic instabilities. Not surprisingly, the conduction band primarily has V 3d character, whereas the valence band has O 2p character. Electron localization at specific V 3d states on the V_2O_5 framework can create a small gap near the first peak of the conduction band in proximity to the Fermi level, thereby providing one possible pathway for a metal–insulator transition. The localization may be facilitated by local structural distortions and/or Coulomb correlations of d electrons. Another possible alternative that can be envisaged is that deviation from perfect stoichiometry ($x < 0.33$) (or p-doping) may lead to occupation of the in-gap state but not

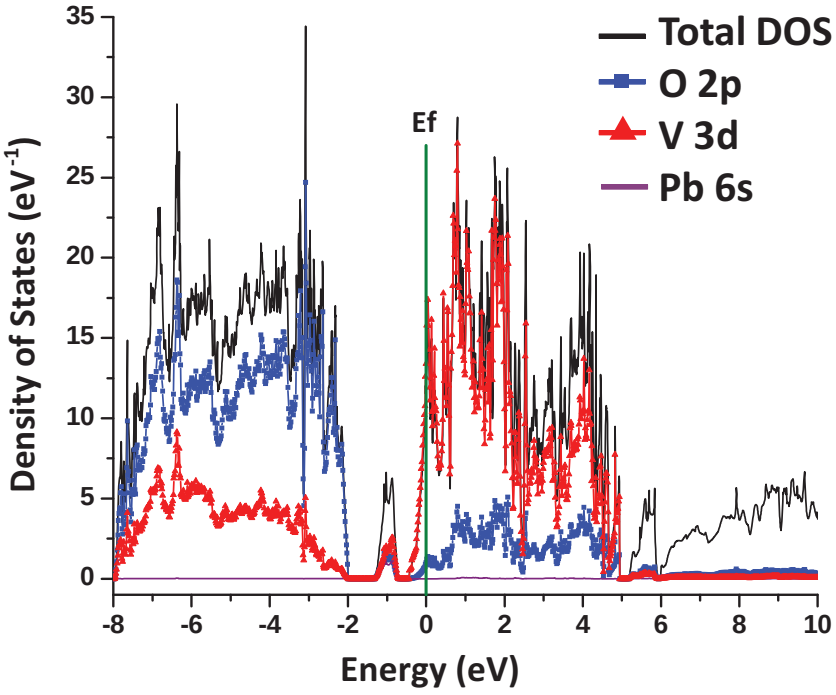

Figure 3. Caclulated density of states for β-$Pb_{0.33}V_2O_5$ showing the total DOS (black), contributions from O 2p (blue squares), V 3d (red triangles), and Pb 6s (solid purple line). The Fermi level is defined as 0.0 eV and a green line is shown for clarity.

the conduction band, thereby rendering β-$Pb_xV_2O_5$ a small gap insulator or poor metal. Increasing the carrier density, would result in occupation of the conduction band rendering the nanowires metallic in character.

2.4. Metal–Insulator Transitions of β-$Pb_{0.33}V_2O_5$

No pronounced thermally driven metal–insulator transition has been observed for β-$Pb_xV_2O_5$ nanowires in the range between 200–400 K.[9] In a classical strongly correlated Mott insulator, if a certain threshold carrier density can be achieved either through thermal excitation, optical pumping, or application of a voltage/current, bound localized states can no longer be stabilized and an abruptly discontinuous transition to a correlated metallic regime is evidenced with a step change in the free carrier density.[1c] Thermal excitation potentially gives rise to peculiar lattice distortions or generation of random potentials that can preclude observation of a thermally-induced metal–insulator transition for β-$Pb_xV_2O_5$ nanowires. Remarkably, upon application of a voltage to pressed pellets of the nanowires, a pronounced and entirely reversible hysteretic transition to a metallic regime is observed, as indicated in **Figure 4**. Typical values of R at room temperature are 100–800 Ω. In the 200–400 K temperature range, R follows an Arrhenius form $R = R_o\exp[E_a/k_BT]$ (Figure 4a inset), where k_B is Boltzmann's constant and T is temperature. This dependence has been seen previously in other nanoscale vanadium oxide systems.[7b,15b] For our β-$Pb_xV_2O_5$ nanowire pellets, E_a ranges between 85–110 meV.

In Figure 4, starting at the lowest temperature (150 K) the voltage (V) has been driven from zero at a fixed rate and the current (I) through the sample has been measured. At a certain threshold, V_{TH}, a large jump in I signifying induction of an insulator→metal transition is observed. In an effort to protect the sample from Joule heating, I through the sample is limited to 250 mA in all the measurements. In the reverse sweeping direction, another sharp I jump albeit at a voltage value less than V_{TH} is noted, manifesting a hysteresis. As T is increased, the I versus V curves are increasingly broadened and above ≈235 K hardly any hysteresis is discernible. However, a broad MIT is noted even as high as room temperature. The T dependence of V_{TH} can be been fitted to exp $(-T/T_o)$, (Figure 4b), which is characteristic to other strongly correlated materials, and is often suggestive of a charge ordering-induced metal→insulator transition.[16]

An alternative scenario can also be considered based on observations of sharp switching in electrical resistance noted at metal-oxide/metal interfaces, such as for $SrTiO_{3-x}$ or TiO_2, which has been attributed to electroforming processes that facilitate charge transport via the field-directed motion of oxygen vacancies.[17] While the precise details of this phenomena remain to be elucidated, it has been hypothesized that conductive filaments are formed between the metal electrodes through Joule heating processes and that mobile vacancies migrate within this region. As with mechanistic understanding of any chemical process, verification of the correct mechanism is difficult. However, the balance of evidence suggests melting of charge ordering and not electroforming or Joule heating-induced vacancy migration as the underlying origin of the transport behavior observed for β-$Pb_xV_2O_5$ pellets. Notably, such a mechanism and the role of electron correlation have been established for other vanadium oxide bronzes such as β-$Ca_{0.33}V_2O_5$ and β-$Na_{0.33}V_2O_5$ (the latter even showing superconductivity). Furthermore, although not as pronounced as in the nanowires, single crystals of $Pb_xV_2O_5$ do show a thermally induced discontinuity in their electrical transport behavior.[9b] It is reasonable to expect that a mechanism similar to the bulk will be manifested at nanoscale dimensions. Optical microscopy and SEM imaging further do not show characteristic electroforming lines in our pellets even after switching over scores of cycles. Perhaps the most compelling evidence is presented in Figure 4c and parallels measurements by Natelson and co-workers to resolve the role of carrier density versus Joule heating in systems such as the Verway transition of Fe_3O_4. Current flow through narrow hot filaments will produce a significant amount of Joule heating, raising the temperature of the sample to a certain value above that of the set temperature. Thus it is expected that as the set temperature increases, the dissipated power due to Joule heating at the threshold voltage should decrease. However, we observe the opposite trend in our measurements as shown in the power

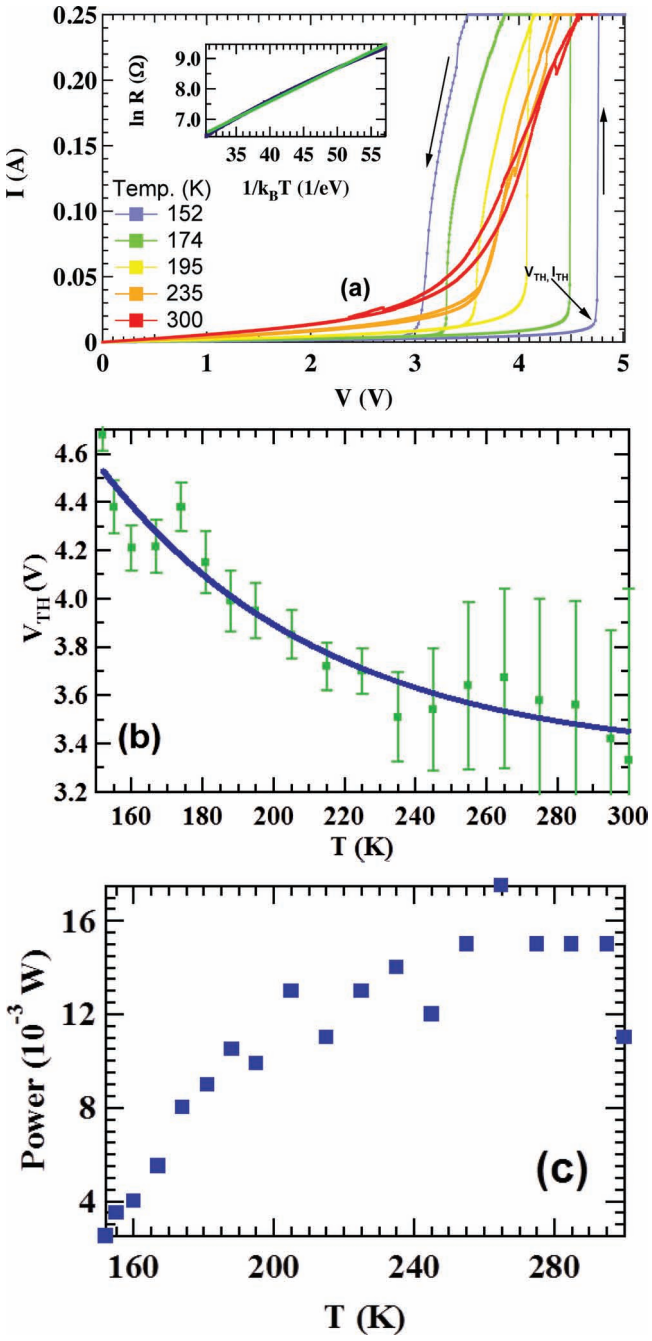

Figure 4. a) Current (I) vs voltage (V) for β-$Pb_{0.33}V_2O_5$ nanowire pellets at different temperatures. Arrows indicate direction of voltage sweeping. Inset: Resistance in log scale vs $1/k_BT$ where k_B is Boltzmann's constant. Green curve shows Arrhenious dependence ~exp[E_a/k_BT]. E_a = 109 meV. b) Threshold voltage, V_{TH}, (indicated in main panel of (a)) vs T. Exponential fit takes the form exp($-T/T_0$). c) Power dissipated at the threshold (V_{TH} I_{TH}) vs temperature.

dissipation curve depicted in Figure 4c, suggesting the likelihood of an electric-field induced transition.[18a,b]

As reported in previous literature, voltage-driven pulse measurements have often been helpful in separating the effects between electric field and Joule heating in driving the MIT in other vanadium oxide systems.[18c,d,e] For such a measurement to be meaningful, the timescales for trigging an electric field-driven transition must be known relative to that of trigging a Joule heating transition; for example, Stefanovich et al. successfully employed a heat balance equation for VO_2 systems to estimate the time required for the temperature of the sample to rise due to Joule heating across the transition temperature (T_c as denoted in VO_2) for given values of dissipated power.[18e] This calculation requires knowledge of the resistivity, specific heat, thermal conductivity and T_c, none of which are currently known for our new system.[19c] Furthermore, very long relaxation behavior in resistance have been observed as V approaches V_{TH}. These effects may be intrinsic to all vanadium systems near the transition and hence applicability of pulsed electrical measurements to vanadium oxide systems near the transition has proven to be rather complex.[19d,e]

While the precise mechanism remains unclear, Pb^{2+} cationic ordering both along the length and across tunnels (verified by the observation of superstructure reflections in the diffraction pattern), the calculated electronic structure depicted in Figure 3, and the charge disproportionation evidenced at room temperature in the NEXAFS measurements suggest that electron delocalization and transformation to the metallic state is induced when the applied electric field generates sufficient free carrier density to melt the specific charge ordering motif of β-$Pb_xV_2O_5$.[15b,19] The unusual V-O-Pb-hybridized in-gap state and the DOS maxima at the Fermi level further corroborate the intrinsic electronic instabilities of this material. These results represent the first voltage-induced metal–insulator transitions observed for classical tunnel-type β/β' Wadsley bronzes and indicate that optically pumping or electrically inducing a threshold carrier density can uncloak a wide variety of eclectic transport phenomena in these materials.

3. Conclusions

The synthesis of single-crystalline β-$Pb_xV_2O_5$ nanowires thus enables interrogation of the intrinsic electronic phase diagram of this material, demonstrating an unprecedented voltage-induced metal–insulator transition along the length of the strongly correlated quasi-1D framework. X-ray diffraction, NEXAFS spectroscopy, and electrical transport data suggest superstructure ordering of cations, and charge disproportionation for the insulating phase; melting of charge ordering likely induces collective electron motion and transformation to the metallic state upon the application of a voltage. An unusual in-gap state is observed in the calculated electronic structure, which along with the DOS maxima at the Fermi level suggests a possible pathway for a carrier-density-dependent phase transformation from a narrow gap semiconductor to a metal. An entirely new class of materials, vanadium bronzes formed with divalent cations, exhibiting sharply discontinuous voltage-induced metal–insulator transitions will be of great relevance for device applications such as memristors, Mott field-effect transistors, and electrochromic coatings.[1c,20] Based on the memory capacitance effect, Basov and co-workers have designed a memory metamaterial device that harnesses the memory effects in the insulator–metal

transition of the canonical metal–insulator transition material VO_2 to yield robust stimuli-responsive frequency-switchability of the electromagnetic response.[20b,21] The ability to adjust the electromagnetic output of an object in real time has tremendous bearing for the field of transformation optics, especially the vaunted goal of electromagnetic cloaking.[22] Vanadium bronzes derived from divalent cations with voltage tunable metal–insulator transitions represent a useful new addition to the sparse roster of materials suitable for this purpose apart from being fundamentally interesting 1D model systems for examination of charge fluctuations and strong correlation.

4. Experimental Section

Powder X-ray diffraction (XRD) data was collected in Bragg-Brentano geometry using a Rigaku Ultima IV instrument (Cu K_α radiation, voltage 40 kV, current 44 mA). The nanowire samples were ground to a fine powder and packed in a sample holder with 0.5 mm depth for the powder XRD measurements. Pattern fitting and phase identification were achieved with the help of JADE 8.5. The morphology of the as-prepared nanowires was evaluated by scanning electron microscopy (SEM, Hitachi SU-70 operated at 25 kV equipped with an X-ray detector), and by combining high-resolution transmission electron microscopy (HRTEM) with selected area electron diffraction (SAED, JEOL-2010, 200 kV, 100 mA). For transmission electron microscopy, the samples were dispersed in 2-propanol using a bath sonicator and then deposited onto 300 mesh carbon-coated Cu grids. Near-edge X-ray absorption fine structure (NEXAFS) data were collected on National Institute of Standards and Technology beamline U7A and X23A2 at the National Synchrotron Light Source (NSLS) of Brookhaven National Laboratory with a toroidal mirror spherical grating monochromator using a 1200 lines/mm grating and an energy resolution of 0.1 eV. NEXAFS data were collected in partial electron yield (PEY) mode with a channeltron multiplier near the sample surface using the detector at –200 kV bias to enhance surface sensitivity. The PEY signal was normalized by the drain current of a clean gold mesh located along the path of the incident X-rays. In addition, all the data was collected along with a standard V reference mesh for energy calibration. V K-edge XANES data were acquired in transmission mode on beamline X23A2 of the NSLS for powder samples of nanowires milled with BN. All spectra were calibrated using a V metal foil, for which spectra were simultaneously collected during all transmission mode experiments. A Si(311) monochromator was used for an overall spectral resolution ($\Delta E/E$) of 2×10^{-4}. High resolution X-ray photoelectron spectroscopy was performed using a Phi 5000 Versa Probe instrument using Mg Kα as the X-ray source.

Redox titrations to determine the valence of vanadium in β-$Pb_xV_2O_5$ nanowires were performed by dissolving a weighed amount of the solid in 20 mL of concentrated H_2SO_4 solution (J.T. Baker) at 50 °C. The resulting solution was first titrated with 0.0104 M $KMnO_4$ (Alfa Aesar) to determine moles of V^{4+} via oxidation to V^{5+}. Subsequently, following titration with $KMnO_4$, a second titration with a 0.0187 M solution of iron(II) ammonium sulfate (Sigma Aldrich) was used to determine the total moles of vanadium. Both sets of titrations were performed in triplicate. Ab initio density functional theory (DFT) as implemented in the Quantum ESPRESSO package was used to determine the atom-projected DOS for β-$Pb_{0.33}V_2O_5$ from first-principles consideration.[23] The generalized gradient approximation was used for exchange and correlation terms along with ultrasoft pseudopotentials to describe the electron–ion interactions.[24]

Acknowledgements

S.B. and S.G. acknowledge support from the National Science Foundation under DMR 0847169 and DMR 0847324, respectively. P.Z. is supported by the National Science Foundation under Grant No. DMR-0946404. S.B. also acknowledges the Research Corporation for Science Advancement through a Cottrell Scholar Award.

Received: June 6, 2012
Published online: August 17, 2012

[1] a) E. Dagotto, *Science* **2005**, *309*, 257; b) M. Imada, A. Fujimori, Y. Tokura, *Rev. Mod. Phys.* **1998**, *70*, 1039; c) L. Whittaker, C. J. Patridge, S. Banerjee, *J. Phys. Chem. Lett.* **2011**, *2*, 745.
[2] a) P. Fulde, P. Thalmeier, G. Zwicknagl, *Solid State Phys.* **2006**, *60*, 1; b) T. Yamauchi, Y. Ueda, *Phys. Rev. B* **2008**, *77*, 104529/1.
[3] a) A. D. Wadsley, *Acta Crystallogr.* **1955**, *8*, 695; b) H. Kessler, M. J. Sienko, *J. Solid State Chem.* **1970**, *1*, 152; c) J. H. Perlstein, M. J. Sienko, *J. Chem. Phys.* **1968**, *48*, 174; d) J. B. Goodenough, *J. Solid State Chem.* **1970**, *1*, 349; e) M. Ganne, A. Jouanneaux, M. Tournoux, A. Le Bail, *J. Solid State Chem.* **1992**, *97*, 186.
[4] a) R. L. Withers, P. Millet, Y. Tabira, *Z. Kristallogr.* **2000**, *215*, 357; b) T. Yamauchi, M. Isobe, Y. Ueda, *Solid State Sci.* **2005**, *7*, 874.
[5] a) H. Yamada, Y. Ueda, *J. Phys. Soc. Jpn.* **1999**, *68*, 2375; b) J. I. Yamaura, T. Yamauchi, M. Isobe, H. Yamada, Y. Ueda, *J. Phys. Soc. Jpn.* **2004**, *4*, 914.
[6] a) S. C. Erwin, L. Zu, M. I. Haftel, A. L. Efros, T. A. Kennedy, D. J. Norris, *Nature* **2005**, *436*, 91; b) D. J. Norris, A. L. Efros, S. C. Erwin, *Science* **2008**, *319*, 1776; c) G. M. Dalpian, J. R. Chelikowsky, *Phys. Rev. Lett.* **2006**, *96*, 226802/1.
[7] a) C. J. Patridge, C. Jaye, H. Zhang, A. C. Marchilok, D. A. Fischer, E. S. Takeuchi, S. Banerjee, *Inorg. Chem.* **2009**, *48*, 3145; b) C. J. Patridge, T. Woo, C. Jaye, B. Ravel, E. S. Takeuchi, D. Fischer, S. Ganapathy, S. Banerjee, *Nano Lett.* **2010**, *10*, 2448; c) C. J. Patridge, T.-L. Wu, G. Sambandamurthy, S. Banerjee, *Chem. Commun.* **2011**, *47*, 4484; d) P. M. Marley, S. Banerjee, *Inorg. Chem.* **2012**, *51*, 5264.
[8] C. Ma, H. X. Yang, Z. A. Li, Y. Ueda, J. Q. Li, *Solid State Commun.* **2008**, *146*, 30.
[9] a) T. Yamauchi, H. Ueda, Y. Ueda, J. Kikuchi, *Phys. C* **2007**, *462*, 532; b) T. Yamauchi, *J. Magn. Magn. Mater.* **2004**, *272–276*, 442.
[10] a) J. Stohr, *NEXAFS Spectroscopy*, Springer, Berlin **1992**; b) J. M. Velazquez, C. Jaye, D. A. Fischer, S. Banerjee, *J. Phys. Chem. C* **2009**, *113*, 7639; c) M. Havecker, A. Knop-Gericke, R. W. Mayer, M. Fait, H. Bluhm, R. Schlogl, *J. Electron Spectrosc. Relat. Phenom.* **2002**, *2*, 79.
[11] O. Mentré, M. Huvé, F. Abraham, *J. Solid State Chem.* **1999**, *145*, 186.
[12] V. Ta Phuoc, C. Sellier, B. Corraze, E. Janod, C. Marin, *Eur. Phys. J. B* **2009**, *181–186*, 00148.
[13] M. Niwa, Y. Murakami, *J. Catal.* **1982**, *76*, 9.
[14] a) J. Wong, F. W. Lytle, R. P. Messmer, D. H. Maylotte, *Phys. Rev. B* **1984**, *30*, 5596; b) T. Yamamoto, *X-Ray Spectrometry* **2008**, *37*, 572; c) P. Chaurand, J. Rose, V. Briois, M. Salome, O. Proux, V. Nassif, L. Olivi, *J. Phys. Chem. B* **2007**, *111*, 5101.
[15] a) J. Wei, Z. Wang, W. Chen, D. H. Cobden, *Nat. Nanotechnol.* **2009**, *4*, 420; b) T.-L. Wu, L. Whittaker, S. Banerjee, G. Sambandamurthy, *Phys. Rev. B* **2011**, *83*, 073101/1.
[16] a) T. Driscoll, H. T. Kim, B. G. Chae, M. Di Ventra, D. N. Basov, *Appl. Phys. Lett.* **2009**, *95*, 043503; b) S. Bogdanovich, D. Popovic, *Phys. Rev. Lett.* **2002**, *88*, 23640; c) A. A. Stabile, L. Whittaker, T.-L. Wu, P. M. Marley, S. Banerjee, G. Sambandamurthy, *Nanotechnology* **2011**, *22*, 485201; d) M. Benzaquen, D. Walsh, *Phys. Rev. B* **1984**, *30*, 7287.
[17] a) W. Jiang, R. J. Kamaladasa, Y. M. Lu, A. Vicari, R. Berechman, P. A. Salvador, J. A. Bain, Y. N. Picard, M. Skowronski, *J. Appl. Phys.* **2011**, *110*, 054514; b) J. J. Yang, F. Miao, M. D. Pickett,

D. A. A. Ohlberg, D. R Stewart, C. N. Lau, R S. Williams, *Nanotechology*, **2009**, *20*, 215201; c) J. P. Strachan, M. D. Pickett, J. J. Yang, S. Aloni, A. L. D. Kilcoyne, G. Medeiros-Ribeiro, R. S. Williams, *Adv. Mater.* **2010**, *22*, 3573; d) Y. M. Lu, W. Jiang, M. Noman, J. A. Bain, P. A. Salvador, M. Skowronski, *J. Phys. D.* **2011**, *44*, 185103; e) W. Jiang, M. Norman, Y. M. Lu, J. A. Bain, P. A. Salvador, *J. Appl. Phys.* **2011**, *110*, 034509.

[18] a) S. Lee, A. Fursina, J. T. Mayo, C. T. Yavuz, V. L. Colvin, R. G. S. Sofin, I. V. Shvets, D. Natelson, *Nat. Mater.* **2007**, *7*, 130; b) A. A. Fursina, R. G. S. Sofin, I. V. Shvets, D. Natelson, *Phys. Rev. B.* **2009**, *79*, 245131; c) B.-G. Chae, H.-T. Kim, D.-H. Youn, K.-Y. Kang, *Phys. B.* **2005**, *369*, 76; d) H.-T. Kim, B.-J. Kim, S. Choi, B.-G. Chae, Y. W. Lee, T. Driscoll, M. M. Qazilbash, D. N. Basov, *J. Appl. Phys.* **2010**, *107*, 023702; e) G. Stefanovich, A. Pergament, D. Stefanovich, *J. Phys,: Condens. Matter.* **2000**, *12*, 8837.

[19] a) K. Maki, *Phys. Rev. B* **1986**, *33*, 2852; b) Y. Taguchi, T. Matsumoto, Y. Tokura, *Phys. Rev. B* **2000**, *62*, 7015; c) A. L. Pergament, G. B. Stefanovich, F. A. Chudnovskii, *Tech. Phys. Lett.* **1993**, *663*, 19; d) J. H. Claassen, J. W. Lu, K. G. West, S. A. Wolf, *Appl. Phys. Lett.* **2010**, *96*, 132102; e) S. Sengupta, K. Wang, K. Liu, A. K. Bhat, S. Dhara, J. Wu, M. M. Deshmukh, *Appl. Phys. Lett.* **2011**, *99*, 062114.

[20] a) T. Driscoll, H.-T. Kim, B.-G. Chae, B.-J. Kim, Y. W. Lee, N. M. Jokerst, S. Palit, D. R. Smith, M. Di Ventra, D. N. Basov, *Science* **2009**, *325*, 1518; b) T. Driscoll, G. O. Andreev, D. N. Basov, *Appl. Phys. Lett.* **2007**, *91*, 062511/1; c) D. M. Newns, J. A. Misewich, C. C. Tsuei, A. Gupta, B. A. Scott, A. Schrott, *Appl. Phys. Lett.* **1998**, *73*, 780; d) F. Chudnovskiy, S. Luryi, B. Spivak, *Future Trends in Microelectronics: The Nano Millenium*, Wiley-Interscience, New York **2002**, 148.

[21] M. Di Ventra, Y. V. Pershin, L. O. Chua, *Proc. IEEE* **2009**, *97*, 1371.

[22] J. B. Pendry, D. Schurig, D. R. Smith, *Science* **2006**, *312*, 1780.

[23] P. Giannozzi, S. Baroni, N. Bonini, M. Calandra, R. Car, C. Cavazzoni, D. Ceresoli, G. L. Chiarotti, M. Cococcioni, I. Dabo, A. D. Corso, S. de Gironcoli, S. Fabris, G. Fratesi, R. Gebauer, U. Gerstmann, C. Gougoussis, A. Kokalj, M. Lazzeri, L. Martin-Samos, N. Marzari, F. Mauri, R. Mazzarello, S. Paolini, A. Pasquarello, L. Paulatto, C. Sbraccia, S. Scandolo, G. Sclauzero, A. P. Seitsonen, A. Smogunov, P. Umari, R. M. Wentzcovitch. *J. Phys: Condens. Matter* **2009**, *21*, 395502.

[24] D. Vanderbilt, *Phys. Rev. B* **1990**, *41*, 7892.